Modeling Ultrafast Laser Ablation on the Glenoid Bone for the Fitting of a Prosthetic Screw

Group 7
BEE 4530

Anya Laibangyang
Allison Liang
Jingyu Wang
Xiaowei Wu

Table of Contents

Executive Summary

In order to fit prosthetic screws, mechanical drilling of the bone has been the norm since the development of modern surgery. However, bone reabsorption, hyperthermia and thermo necrosis could occur depending on the exposure time to the drill and elevated temperature in the surrounding bone due to friction and drill pressure. Non-contact ablation using a CO_2 laser can potentially increase the accuracy of the bone drilling and reduce the amount of friction applied to the bone, thus reducing the thermal effects on the surrounding tissue.

A model of laser ablation of the human glenoid bone was done on COMSOL with a governing equation of transient state heat transfer from laser to bone. This heat transfer was then correlated to bone loss. According to previous studies, bone disintegration occurs at approximately 613 Kelvin. The bone's geometry was simplified to a 2-D axisymmetric cylinder. The two domains of the 5mm deep screw region were also 2D-axisymmetric cylinders with varying radius and depth. The phase field model was used to take into account the ablation process of bone. Because the bone essentially disintegrates into "gas-like" particles after reaching this temperature, the phase field model was used to determine the downward velocity of the "air-bone" interface. An adaptive mesh was also developed to move in conjunction with the moving interface.

The laser pattern consisted of consecutive concentric cylindrical shells, with the first pulse at the center of the targeted ablated site and the following pulses were cylindrical shells of increasing area. However, because the radial scanning speed was extremely small compared to the pulse duration, concentric cylindrical shells were assumed to occur simultaneously, creating a constant area of laser ablation for each of the two screw domains. Because the CO_2 laser did not have a significant penetration depth as the heat generated by the laser was absorbed mainly at the bone surface, input laser heating was modeled as constant flux. Finally, the modeling results for laser ablation were compared to factors in mechanical bone drilling.

By varying the input flux of the laser within a range of 300 W/cm^2 to 1200 W/cm^2 and measuring the total ablation time and the total damage in the surrounding tissue, an optimal flux range between 1050 W/cm^2 and 1100 W/cm^2 was found to minimize the end time (approximately 0.55 seconds) and thermal damage to the surrounding bone (3.5 mm^3). Compared to mechanical drilling, laser ablation with the optimized flux value was much faster than mechanical drilling which can drill at approximately 0.33 mm per second.

Generally, less surgery time decreases a patient's risk when under anesthesia. An increased amount of thermal damage may also lead to refractures, loosening of the prosthetic and permanent loss of tissue function. As laser ablation minimized both these parameters, this model demonstrates that laser ablation of bone is a viable method to consider in future surgical orthopedic work.

Introduction

Orthopedic surgery is one of the most invasive types of surgery that a patient can have. There has been a constant push for advancement towards finding new methods that either decrease the amount of time required for open surgery or even eliminate the need for a patient to be under the knife. A possible novel method in development is the use of ultrafast laser ablation onto hard bone via patterned laser pulses. Laser ablation is currently used for soft biological tissue and has been experimentally tried on animal hard bones. An important biomedical application of laser ablation is in the field of prosthetics, when holes must be drilled in bones for fitting of prosthetic screws.

In orthopedics, drilling a hole in bone to fit a screw is a technique frequently required for many surgical procedures. For a shoulder replacement, a humoral head implant is placed into the shoulder. A glenoid implant is then required to be placed into the glenoid vault by surgical screws; this implant would provide stability of the humoral head implant and prevent any bone damage on the glenoid vault (Frich, 2007). Drilling holes for fitting these screws are needed in such surgeries. The conventional way of drilling a hole in bones is performed by using mechanical burr drills. Mechanized cutting tools have relatively high speeds: 10,000- 400,000 rpm in dental applications, and up to 1000 rpm in orthopedic procedures (Bertollo & Walsh, 2011). These high speeds can cause thermal necrosis in bone, thus producing undesired bone mass loss. Other complications associated with mechanical burr drills include micro fractures in the adjacent bone tissue and relatively low ablation accuracy. Most of these injuries can be attributed to the friction and pressure caused by the drill's contact with the bone. Lasers have been shown to be a promising alternative to mechanical tools. By producing high-energy light-tissue interactions in a focused area, lasers are able to perform precise non-contact ablation (Bertollo & Walsh, 2011). Using laser ablation in bone can eliminate the need for manual drilling, and thus this can decrease possibility for human error made by a surgeon.

The general process of laser ablation involves raising molecules to an excited state by absorbing light photons. Molecules then return to ground state by photon emission or via molecular vibrations, which produce thermal energy. Absorption of electromagnetic radiation in bone determines specific laser characteristics that must be used for ablation. Main absorbents in bone are water and collagen fibrils, but absorption also occurs in calcium and phosphate apatite. However, electromagnetic absorption peaks for bone can shift during tissue preparation and laser ablation due to changing thermal conditions. Because of these constantly changing factors, it is at times difficult to apply in vitro experimental findings to in vivo applications.

Lasers were introduced for clinical use in the 1960s, and its first applications on hard tissue ablation were in the field of dentistry in 1964 (Emigh, 2011). Continuous waves and pulsed laser methods were considered in dental tissue removal. However, it was not until the 1980s that laser ablation was tried on bone (Emigh, 2011). Early studies focused on long-pulsed laser in the infrared region, but such techniques are capable of producing fractures adjacent to the irradiated regions (Emigh, 2011). Because of this, conventional mechanical drilling had been the dominant method in prosthetic surgeries for a long time. Recently, with the improvements of pulse amplification and other laser technologies, ultrashort laser pulses have becomes accessible to the medical field.

According to Niemz the ablation efficiency of bone is closely related to the laser irradiance (Niemz, 1996). There are two strategies generally employed to achieve high ablation efficiency: a lower flux in combination with a longer ablation time or a higher flux in

combination with a shorter ablation time. Ultrafast laser ablation, which utilizes the second strategy, is a promising tool in orthopedic procedures because it is able to produce precise ablation results and limited thermal damage to the surrounding tissues.

Current research shows that there are minimal thermal and mechanical damages through laser pulsing on the bone. Femtosecond pulses allow the maintenance of the Phosphorus to Calcium ratio in bone at the ablation site. If the ratio changes, there would be a localized change in pH that would delay the overall tissue healing. Another benefit of this ablation method is that the mechanical and photo acoustic stresses are so small that their effects are negligible to the bone. Thus, ultrafast laser ablation on bone is a promising alternative method in orthopedic surgery. One application would be the creation of a hole in a bone for the placement of a screw, specifically a screw holding a prosthetic in the glenoid. In total shoulder anthroplasty during which a total shoulder replacement takes place, the glenoid is fitted with prosthetics to ensure the success of the implant. In current procedures, holes are drilled into the glenoid in order to allow the installation of the prosthetic held in place by surgical screws (Frich et. al., 1997). Laser ablation to create the same hole is promising alternative to the mechanical drilling of the hole. A computer model will be made to illustrate the process of laser pulsing onto a human glenoid, to create a hole with dimensions that are tailored to fit a surgical screw.

The goal of this project is to minimize the time taken to ablate a hole fitted for a screw and the amount of thermal damage in the surrounding bone. Analyzing the temperature change in relationship to the mass loss demonstrates the extent to which this procedural laser ablation can be applied. To determine the viability of this procedure in a real-world surgical setting, parameters of our laser ablation method will be compared with that of a mechanical bone drilling method. Parameters considered include total run time of method and amount of thermal damage in surrounding tissue at the end of the ablation time.

Design Objectives:

In this project, a realistic COMSOL computation model of laser ablation of bone will be developed. By varying the flux provided by the laser source, the total ablation time and thermal damage to the surrounding tissue will be monitored and optimized. The model will also be analyzed with respect to specific modeling parameters to determine the sensitivity of the model and thus its overall validity.

Schematic

In COMSOL, the computational domain included the desired ablated area and the surrounding bone region. The model was constructed based on logical assumptions regarding the glenoid bone and screw. The glenoid bone is a relatively flat and smooth surface which leads to the assumption that laser ablation was done on a completely flat surface. The desired ablated area was constructed to be able to the fit the screw in the bone. Because the general screw shape is cylindrical, the ablated region will be cylindrical. Because the shape is symmetrical about a central axis, the COMSOL computations were conducted in a 2D axisymmetric domain as seen in Figure 1 below. Dimensions of ablated region were determined based on relatively real-life screw dimensions in which the screw is 5 mm deep with the head being slightly larger and shallower than the thread. The surrounding bone region was constructed in order to allow observance of any thermal injury that may occur.

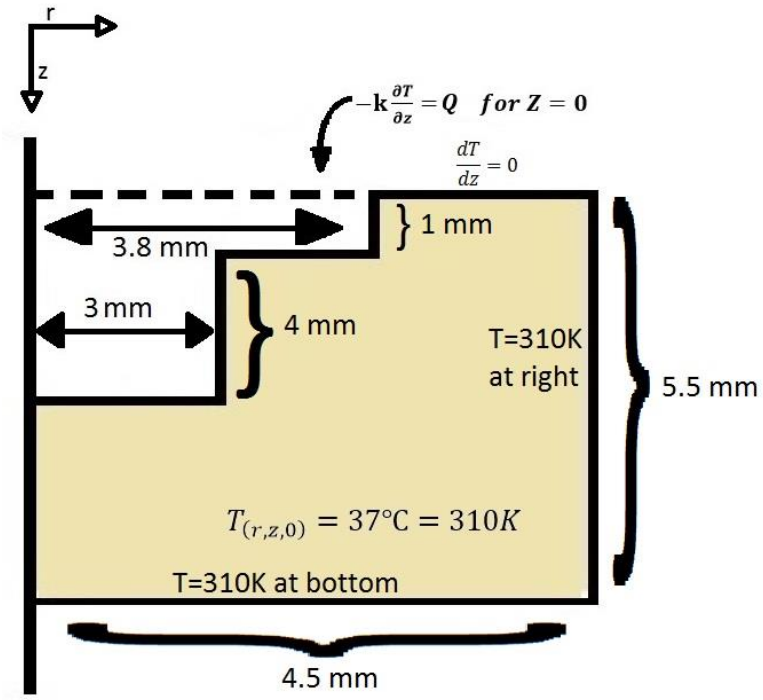

Figure 1: Schematic of the 2-D axisymmetric cylindrical model consisting of two computational domains: the ablated region and the surrounding tissue. The ablated region dimensions were based upon the fitting the glenoid screw into bone. Laser pulses are applied on the bone's top surface at the dotted line boundary. Surrounding tissue region is encloses the area for maximal thermal injury.

Along with the specified dimensions in the schematic above, boundary and initial conditions are also provided in the diagram. For simplicity, all sides of the model are thermally insulated except for the desired laser ablation region. Thus, only heat generation from the laser pulses is considered. All tissue is initially assumed to be at room temperature of 310K.

As the bone surface is exposed to laser pulses, a thin layer of the bone is removed from the air-bone interface separating the two regions (seen as a light blue band in Figure 2 below). As

the bone is ablated, the boundary between the bone and the air moves downward in the z-direction.

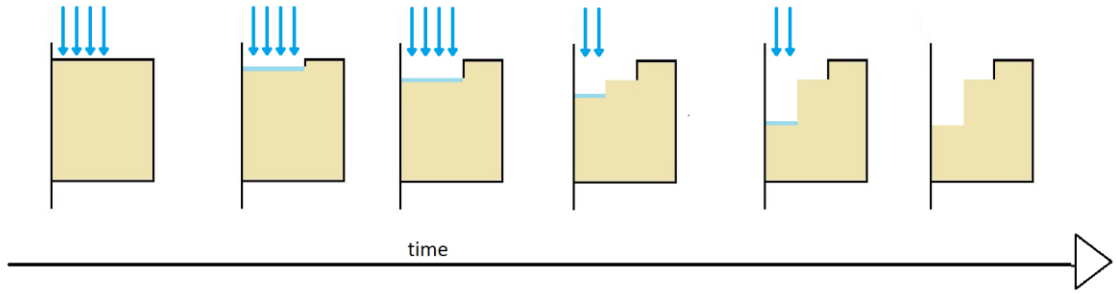

Figure 2: Diagram illustrating the laser ablation process over time for the specified COMSOL model of the glenoid bone. Time increases as the image moves from left to right. The heating of the bone causes an air-bone interface (in blue) to form. As ablation is completed in the first domain of the screw, the width of the point flux decreases and the air-bone interface continually moves down.

At first, the laser pulses have a radius of 3.8mm to create a 1mm hole. The radius of the laser pulses is then readjusted to 3mm and the ablation processes is then continued for an additional depth of 4mm in the z-direction. Figure 2 above illustrates this entire process.

Governing Equations and Boundary Conditions:

In this laser ablation, an increase in temperature leads to the disintegration of bone. Thus the overall governing equation is based on mass loss:

$$\frac{dm}{dt} = \frac{\partial m}{\partial T} \times \frac{\partial T}{\partial t} \qquad (1)$$

In a previous study conducted by Lozano, the relationship between temperature and bone mass loss was determined (Lozano, 2003). They studied temperatures between a range of 0°C to approximately 850°C. Their results are shown below (Figure 3):

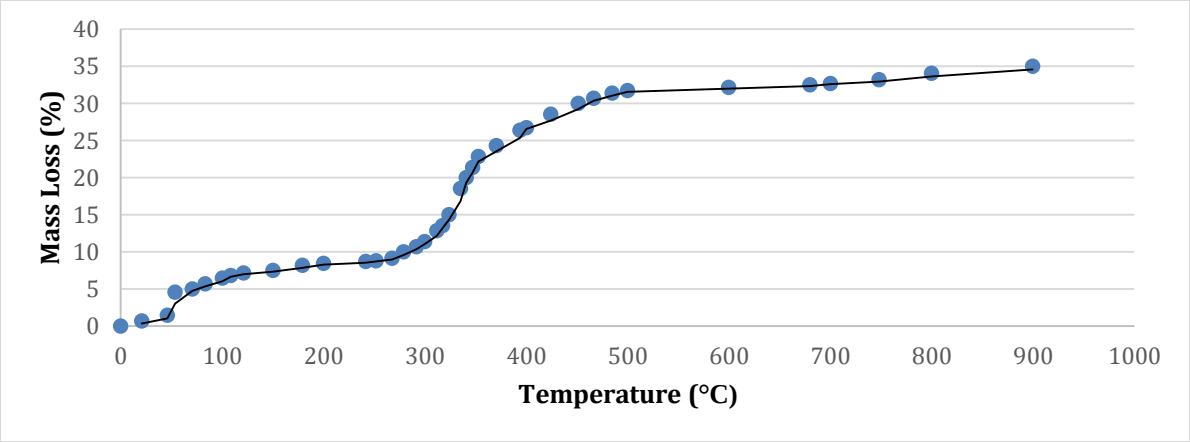

Figure 3: Plot of percent mass loss in bone versus degree Celsius temperature. The plot was obtained from the paper written by Lozano (Lozano, 2003). TGA measurements were carried out in a Thermal Analysis System 9900, Du Pont 951 (TGA module). For TGA measurements the heating rate was constant and equal to 10℃/min in an air atmosphere. The sample amounts used were 20 mg for all cases in TGA experiments.

Figure 3 displays the relationship between an increase in temperature and the total percent of mass loss in bone (Lozano, 2003). The figure shows mass loss up to around 60%. No further mass loss is shown because most of the mass left is the inorganic material, such as hydroxyapatite crystals. Because of their thermal properties, these crystals will only disintegrate at extremely high temperatures that cannot be reached through laser ablation. However the crystal sizes are small enough that they can be easily removed through possible methods such as irrigation. Thus, it is sufficient to only analyze bone mass loss of up to 60%.

Plotting these points in COMSOL, we get a relationship between mass loss and temperature g (T). We can then relate this to equation (1) with the following relationship which we can use in COMSOL:

$$\frac{\partial m}{\partial T} = g(T) \times \frac{M_x}{100} \tag{2}$$

The change in mass over time is also dependent on the change in temperature over time. The change in temperature over time is given by this equation that will be solved by COMSOL.

$$\frac{\partial \mathrm{T}}{\partial \mathrm{t}} = \frac{k}{\rho C_p}\left[\frac{1}{r}\frac{\partial}{\partial \mathrm{r}}\left(\mathrm{r}\frac{\partial \mathrm{T}}{\partial \mathrm{r}}\right) + \frac{\partial^2 \mathrm{T}}{\partial \mathrm{z}^2}\right] + \frac{Q}{\rho C_p} \tag{3}$$

In equation (3), $\frac{k}{\rho C_p}$ is the thermal diffusivity, k is the heat conductivity, ρ is the density, C_p is the specific heat of the bone.

Given that mass is a product of density and volume, equation (1) can be rewritten as:

$$\frac{d\rho V}{dt} = \frac{\partial m}{\partial T} \times \frac{\partial T}{\partial t} \tag{4}$$

$$\frac{dV}{dt} = \frac{\partial m}{\partial T} \times \frac{\partial T}{\partial t} \times \frac{1}{\rho} \quad (5)$$

As the change in volume is the product of area and velocity, another substitution was made giving us:

$$A \times v = \frac{\partial m}{\partial T} \times \frac{\partial T}{\partial t} \times \frac{1}{\rho} \quad (6)$$

Rearranging this in terms of velocity, our governing equation is:

$$v = \frac{\partial m}{\partial T} \times \frac{\partial T}{\partial t} \times \frac{1}{A\rho} \quad (7)$$

For equation (3), we have the boundary conditions and initial conditions listed below:

Initial Condition #1 $T(t=0) = T_i = 310$ K (8)

Boundary Condition #1 as $r \to \infty$, $T(r) = 310$ K (9)

Boundary Condition #2 as $z \to \infty$, $T(z) = 310$ K (10)

Boundary Condition #3 $\frac{\partial T}{\partial r}|_{r=0} = 0$ (11)

Boundary Condition #4 $k\frac{\partial T}{\partial z}|_{z=0} = Q$ (12)

The initial conditions and boundary conditions listed above in equations (8) through (12) are also depicted in the schematic in Figure 1.

To account for when the bone region undergoes ablation, the phase field equation was implemented (appendix A). With this equation, the three regions were accounted for: the air layer, the bone layer, and the air-bone interface. At the interface, the phase field model assumes that the bone material is undergoing a solid to gas phase change. This was an accepted approximation for the ablation process because the disintegrated bone particles are so miniscule that after ablation, air occupies the majority of the region. The previously derived velocity of ablation in the z-direction was implemented as a parameter in the phase field equation (appendix A, equation 7). Thus, coupling the phase field equation with this velocity allows successful idealization of the real-life laser ablation process.

Results and Discussion

From Figure 3, it was interpolated that bone ablation occurs at 613K. As the laser flux is applied, the region where 613K was reached is considered to be ablated and only air remains. Thus, the total air in the bone domain observed is correlated to the areas that have reached ablation temperature. Figure 4 below displays the correlation between temperature (left) and mass loss (right). This figure displays the temperature and air fraction distributions at a time of 0.455 seconds for a 750 W/cm^2 applied flux.

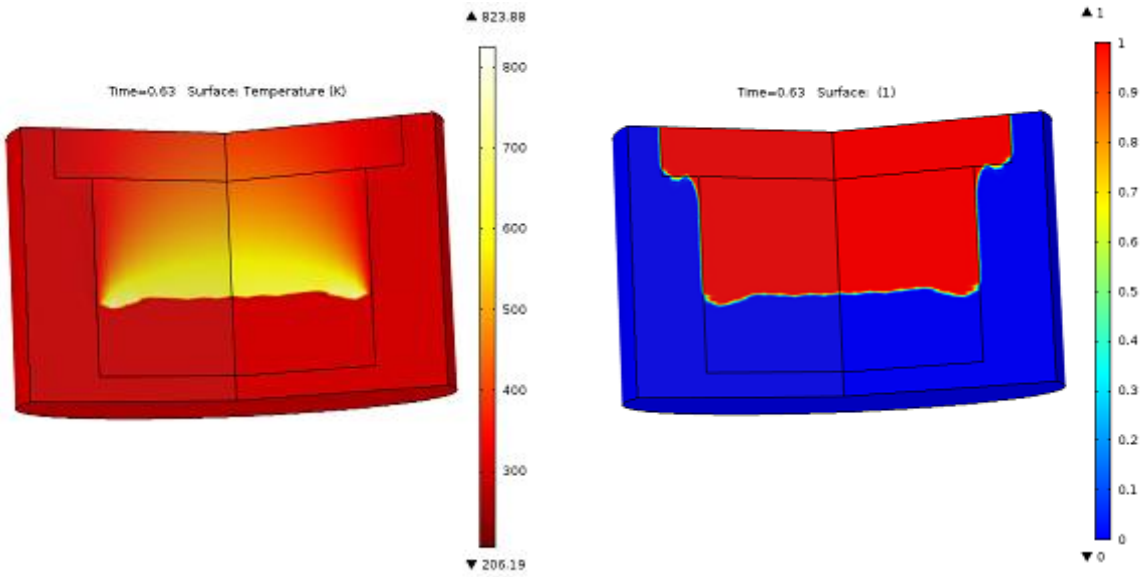

Figure 4. Surface temperature plot of the computational domain (left) and the corresponding surface air fraction volume plot (right) at t= 0.455 seconds. The two plots combined shows the moving air-bone interface and the relationship of temperature to mass loss in bone. A flux of 750 W/cm^2, a surface tension of 1 N/m, a mobility of 1 m·s/kg and a total element distribution of 960 elements were used.

The surface plot on the left is for temperature distribution. At the time of 0.455 seconds, the plot shows that the highest temperature (the yellow region) is around the center of the desired ablated domain, which implies that the air-bone interface is also located near the center. The temperature color scale shows that the light yellow to white colors indicate that the temperature in that region is above 613K, which is seen at the air-bone interface. Because the model starts with flux applied at top of the desired ablated domain, the surface plot signifies that all area that is above the location of the interface has reached 613K previously. Thus, this whole region is ablated and only air is present as seen on the right plot in Figure 4; the air volume fraction distribution across the bone domain is illustrated in a surface plot. The color scale for the air volume fraction indicates that the color red represents air volume fraction as one and thus no bone is present. This surface plot displays the same results found in the temperature surface plot shown on the left in Figure 4. As previously stated, any part of the targeted region that is above the current yellow area in the temperature surface plot has already been ablated. In the air volume fraction surface plot, the red region is at the same specified location range as the determined ablated region from the temperature plot. It is concluded that regions with an air volume fraction of one represents bone that has reached 613K and was ablated. Thus, ablation process is correctly represented in the COMSOL model and air fraction volume distributions can be used to accurately observe bone ablation.

The laser ablation process specified for the model was ran at fluxes ranging from 300 to 1200 W/cm^2. Fluxes were ran at 300, 600, and 750 W/cm^2. From 750 to 1200 W/cm^2, fluxes were run at increments of 50 W/cm^2. From these models, a relationship between applied laser flux and time for the complete ablation of the target domain (end time) was derived. Figure 5 provides a plot of total ablation time with respect to flux.

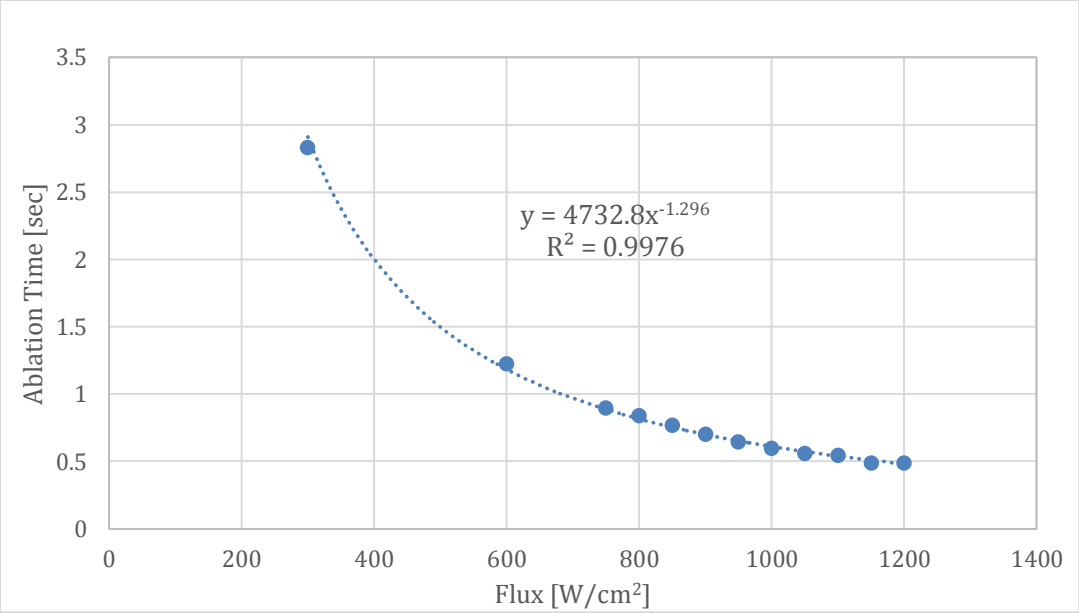

Figure 5. Plot of ablation time versus various flux values. A surface tension of 1 N/m, a mobility of 1 m·s/kg and a total element distribution of 960 elements were used.

The above plot shows that the end time data follows a negative power law. The exact power law equation is provided on the graph. The r-squared value (0.9976) indicates that the data follows extremely closely to the interpolated equation. The trend that the data shows is that once a certain flux is reached, any increase in flux after that will only cause a relatively small change in end ablation time. Based on the plot, this starts to occur after the 1000 W/cm^2 is reached. Fluxes above 1000 W/cm^2 correspond to an extremely small ablation time of 0.5 seconds. Thus in a physical sense, the applied flux would look like an instantaneous laser pulse applied on the bone. Such minimal ablation time is advantageous in surgical procedures, but before such a large applied flux can be accepted, thermal injury of the surrounding tissue must be observed.

The rate that the surrounding tissue was converted to total air volume was observed. As shown previously, bone that reaches a temperature 613K is considered to be ablated and in the model, this corresponding region has an air fraction volume of one. Thus, to observe the rate of surrounding tissue ablation, the air fraction volume in the surrounding domain was integrated for each time step throughout the ablation process. Plots of the air fraction volume in the surrounding domain over time were made for each varying flux model, and it was observed that each data plot was roughly linear (appendix C1). Thus, the slopes found from such linear approximations were considered to be the rate of surrounding tissue ablation. Figure 6 below represents all such rates found in each varying flux model. Exact end times for each corresponding flux are also provided for reference.

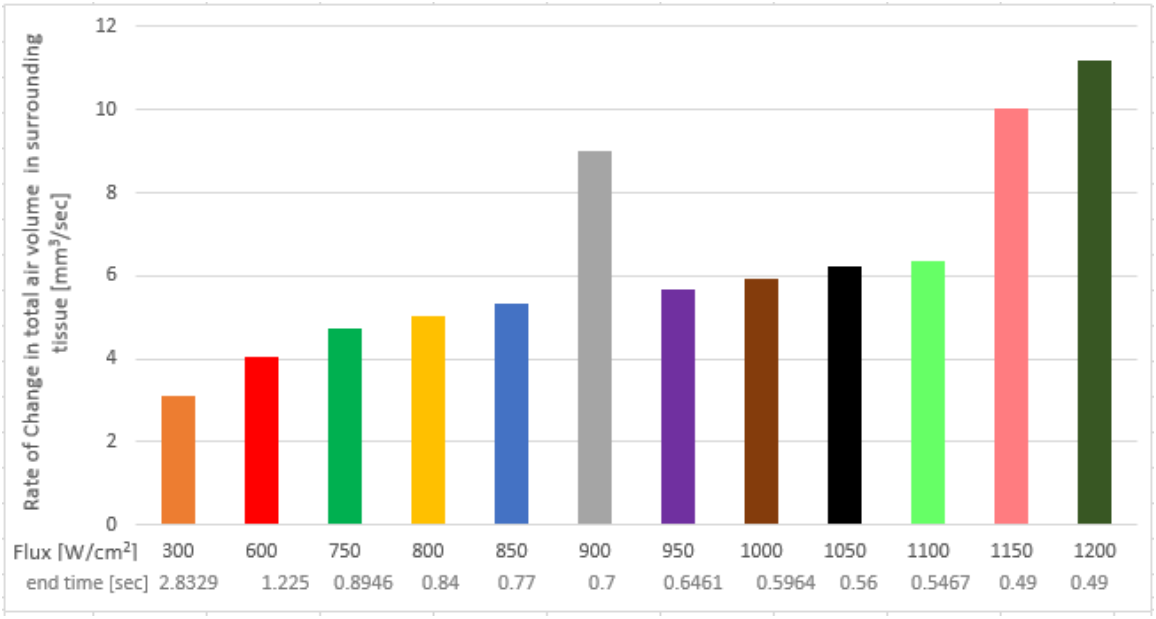

Figure 6. Plot of rate of change in total air volume in surrounding tissue versus various flux values at respective ablation end times. A surface tension of 1 N/m, a mobility of 1 m·s/kg and a total element distribution of 960 elements were used.

In this chart, it appears that with an exception of the 900 W/cm^2 ablation model, the rate of ablation in the surrounding tissue increases as the applied laser flux value increases. This was as expected in that a larger applied laser flux causes the bone to be exposed to larger amounts of heat. Thus, more heat is available to transfer into the surrounding bone domain.

As previously acknowledged, the surrounding tissue ablation rate for a 900 W/cm^2 applied laser flux does not follow the trend that the rates of the other flux models do. This rate found for the 900 W/cm^2 model is shown in Figure 6 as an abnormal spike that is surrounded by rates following a slow increase as the flux magnitude increases. Computational error can be speculated as the cause for such results. However, such error appears to only be occurring in the surrounding region. Referring back to Figure 5, the end time results for the 900 W/cm^2 flux do follow with the observed pattern of end time changing in respect to varying flux. Thus, there is no computational error occurring in the ablated bone region and only results regarding the surrounding thermal injury were affected by this error.

The effects of these surrounding tissue ablation rates are dependent upon the bone domain's exposure time to the specified laser. In the model, exposure time is equivalent to the end time for ablation; the bone is only exposed to the laser when the targeted bone domain is getting ablated. Total air volume in surrounding tissue at the end times of each corresponding flux are displayed in Figure 7.

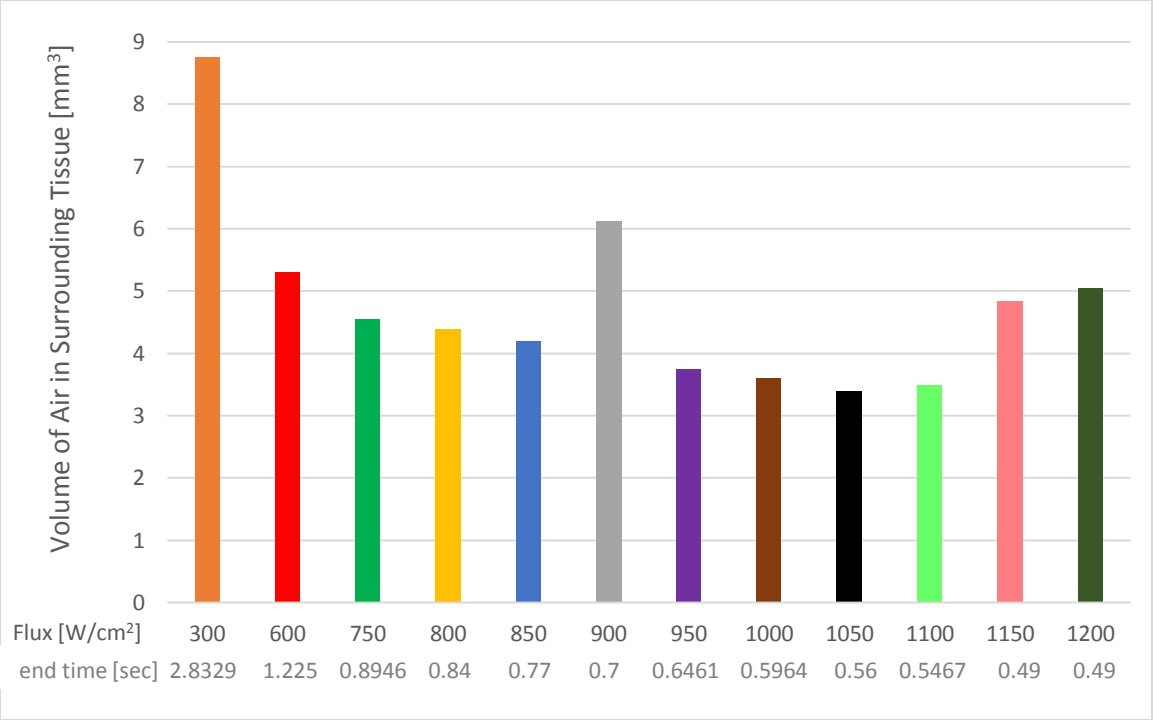

Figure 7. Plot of total air volume in surrounding tissue versus various flux values at respective ablation end times. A surface tension of 1 N/m, a mobility of 1 m·s/kg and a total element distribution of 960 elements were used.

Overall, with the exception of the 900 W/cm^2 model, Figure 7 shows how a general trend of air volume in surrounding tissue follows when increasing the magnitude from 300 to 1200 W/cm^2 of the applied laser flux. Initially at 300 W/cm^2, the air volume in the surrounding tissue is relatively high in respect to the air volume present at higher flux values. This can be attributed to the fact that the exposure time of 2.8329 seconds at 300 W/cm^2 is much longer than the other observed exposure times. The second largest exposure time is 1.225 seconds and this is when the applied flux is 600 W/cm^2. As observed in Figure 7, the air volume in the surrounding tissue shows a clear decrease from that of the 300 W/cm^2 and corresponds to the fact that exposure time has been also decreased as seen in Figure 5. This air volume in the surrounding tissue continues to decrease as the flux increases from 300 to 1050 W/cm^2, again disregarding the results from the 900 W/cm^2 model. When 1050 W/cm^2 laser flux is applied, the exposure time has been dramatically reduced to 0.56 seconds, which was previously observed in Figure 5. At the fluxes past 1050 W/cm^2, the trend in total air volume in surrounding tissue changes and this volume begins to increase as the flux values increase. At an applied laser flux of 1200 W/cm^2, the amount of air in the surrounding tissue is close to the amount of air in the surrounding tissue when the applied laser flux is 600 W/cm^2. This change in air volume trend at 1050 W/cm^2 represents how there is a point at which increasing the laser flux magnitude will begin to cause a noticeable rise of the air volume in the surrounding tissue. Overall, the two factors to be considered when observing ablation in the surrounding tissue are exposure time and the magnitude of the applied laser flux. There was an optimal range of laser fluxes where minimal ablation of the surrounding tissue is achieved. At this range, there is a delicate balance between exposure time and laser flux magnitude. The results represented in Figure 7 suggest that the optimal range for laser flux is between 1050 W/cm^2 and 1100 W/cm^2.

Sensitivity Analysis

The default surface tension and mobility coefficient values are both 1 N/m and 1 m•s/kg, respectively. To test the sensitivity of the model to surface tension coefficient, values were varied to 0.1 and 10 N/m while maintaining a flux of 750 W/cm^2 and a mobility coefficient of 1 m•s/kg. Sensitivity of the mobility coefficient in the model was then tested by varying values to 0.1 and 10 m•s/kg while maintaining the surface tension coefficient as 1 N/m and flux as 750 W/cm^2. These parameters are only relevant with respect to modeling the ablation process in COMSOL and they do not have an effect on real-life experimentation. These models were tested for sensitivity by analysis of two factors: exposure time and total air volume in the surrounding tissue. Figure 8 represents the total ablation time for each varied surface tension and mobility model.

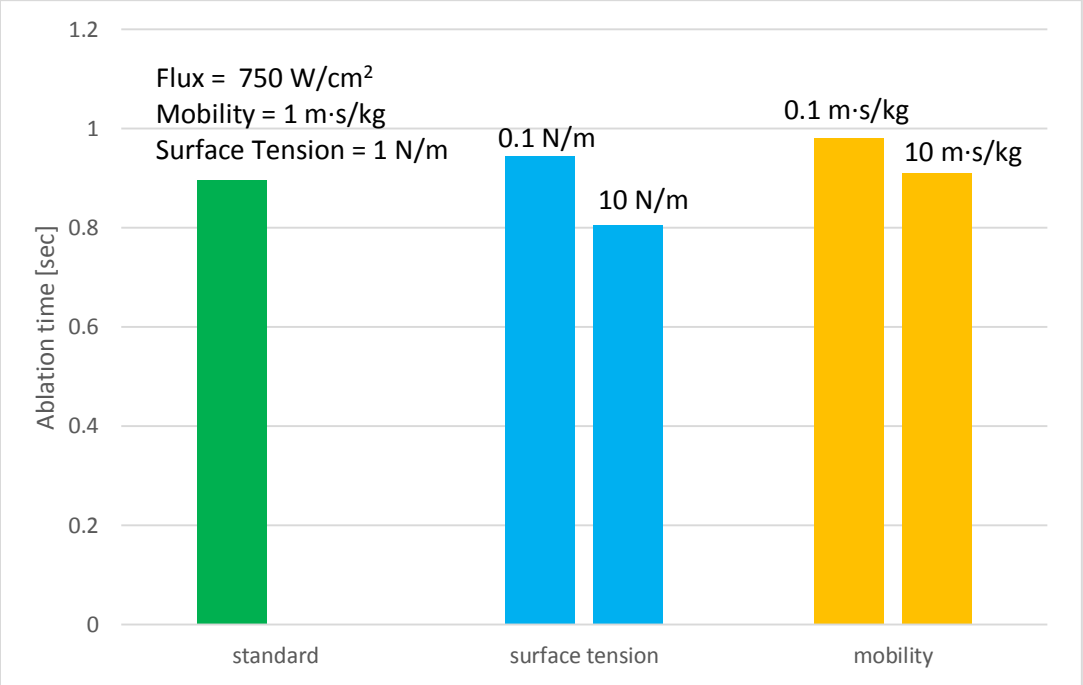

Figure 8. Bar graph of ablation time for various combination of surface tension coefficient values and mobility coefficient values. For the standard model in green, a flux of 750 W/cm^2 , a surface tension of 1 N/m, a mobility of 1 m•s/kg and a total element distribution of 960 elements were used. For the "surface tension group" in blue, a surface tension of 0.1 N/m and 10 N/m were used respectively while maintaining the other parameters as the standard model; for the "mobility group" in orange, a mobility of 0.1 m•s/kg and 10 m•s/kg were used respectively while maintaining the other parameters as the standard model.

The green bar represents the standard model with parameters previously specified. As the surface tension coefficient is varied to 0.1 N/m and 10 N/m, the ablation times vary within a +/- 0.2 second range. Thus, this coefficient was not particularly sensitive with respect to measured ablation end times. Similar results were seen when varying the mobility coefficient. The change also remained within a +/- 0.2 second range and thus the mobility coefficient was also not sensitive with respect to ablation time. Figure 9 demonstrates how sensitive the surface tension

and mobility coefficients are with respect to the surrounding damage in the bone caused by laser ablation.

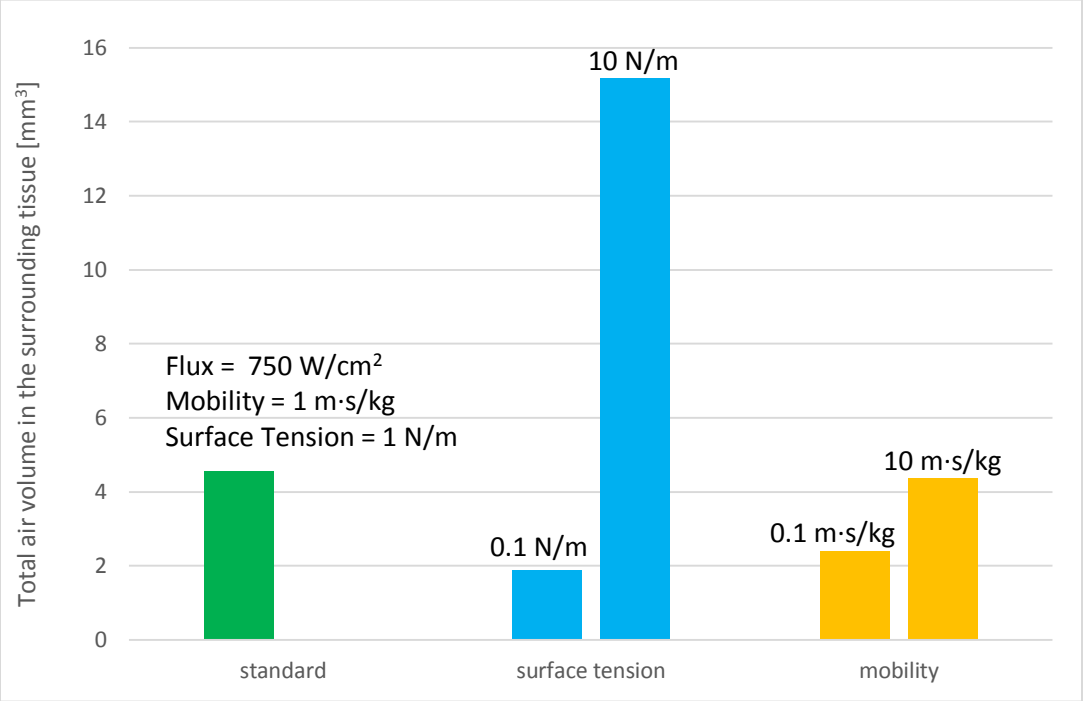

Figure 9: Bar graph of total air volume in surrounding tissue for various combination of surface tension coefficient values and mobility coefficient values at their respective ablation end times. For the standard model in green, a flux of 750 W/cm^2 , a surface tension of 1 N/m, a mobility of 1 m•s/kg and a total element distribution of 960 elements were used. For the "surface tension group" in blue, a surface tension of 0.1 N/m and 10 N/m were used respectively while maintaining the other parameters as the standard model; for the "mobility group" in orange, a mobility of 0.1 m•s/kg and 10 m•s/kg were used respectively while maintaining the other parameters as the standard model.

The green bar represents the standard model at the same specified parameters as that in Figure 8. When decreasing the surface tension coefficient value to 0.1 N/m, there appears to be a clear decrease in the total air volume present in surrounding tissue. When increasing the surface tension coefficient to 10 N/m, there is a large increase in total air volume; the volume is about 15 mm^3 while the standard volume is about 4.2 mm^3. The changes observed when decreasing and increasing the surface tension coefficient indicates that this value is relatively sensitive to the specified model. However, because the surface tension coefficient is only a model used in COMSOL, this observed level of sensitivity has no implications in the real-life experimentation.

Changing the mobility coefficient, in relative to changing the surface tension coefficient, did not cause the total air volume in surrounding tissue to vary much from the standard model results. When the mobility coefficient value is 0.1 m-s/kg, the volume is only smaller by approximately 2 mm^3 and when the value is 10 m-s/kg, the volume is almost identical to the standard volume. Thus, the mobility coefficient is not extremely sensitive in respect to the specified model.

Accuracy Check

Due to the computational limit of COMSOL, the laser was modeled as a continuous point flux rather than in a concentric circle laser pattern mentioned in the ultrafast laser paper (Emigh, 2011). Therefore, literature correlating laser and pulse duration was studied to verify the model. In Ivanenko's and Hering's experiment, a depth per pulse of 8.5 μm is obtained at the fluence of 1.4 J/cm^2 and the frequency of 327 Hz (Ivanenko & Hering, 1998). Thus according to their fluence and frequency, the flux used in their experiment can be calculated.

$$flux = fluence \cdot frequency = 1.4\,\frac{\text{J}}{\text{cm}^2} \cdot 327\ \text{Hz} = 457.8\ \text{W}/cm^2$$

For a hole with a depth of 5 mm, Ivanenko's and Hering's experiment completed the ablation in the time calculated below.

$$Number\ of\ pulses\ N\ = \frac{depth\ of\ bone\ region}{depth\ per\ pulse} = \frac{5\ mm}{8.5\ \mu m} = 588\ pulses$$

$$duration\ time\ for\ ablation\ t = \frac{N}{f} = \frac{588}{327 s^{-1}} = \ 1.799\ s$$

Thus, according to their experiment and laser flux, 1.799 seconds would be needed to ablate a 5mm hole. According to the result obtained from the model in Figure 5, $y = 4732.8 \cdot x^{-1.296}$ where y represents the ablation time and x represents the laser flux. Plugging in the flux of 457.8 W/cm^2 into the equation gives: $y = 4732.8 \cdot 457.8^{-1.296} = 1.686\ s$.

In comparison, 1.686 seconds and 1.799 seconds are extremely close and vary by a minor 6.27%. This small difference shows that the model is relatively accurate in estimating the end time based on the flux values.

Objective Function

Since achieving maximum bone removal at the expected ablated area with minimum bone removal at the surrounding areas is the goal of the project, the following objective function is developed:

$$F_{end\ time}\ (t_i) = \begin{cases} 300 & t \geq 1 \\ 100 & 0.5 \leq t < 1 \\ 0 & t < 0.5 \end{cases} \quad \begin{cases} 300 & t \geq 1 \\ 200 & 0.75 \leq t < 1 \\ 100 & 0.5 \leq t < 0.75 \\ 0 & t < 0.5 \end{cases}$$

$$F_{surrounding\ bone}(Vtot_j) = \begin{cases} 1000 & Vtot \geq 6 \\ 800 & 4.75 \leq Vtot < 6 \\ 500 & 3.5 \leq Vtot < 4.75 \\ 100 & 2.25 \leq Vtot < 3.5 \\ 0 & Vtot < 2.25 \end{cases}$$

$$J = \sum_i F_{end\ time}\ (t_i) + \sum_j F_{unablated\ bone}\ (Vtot_j)$$

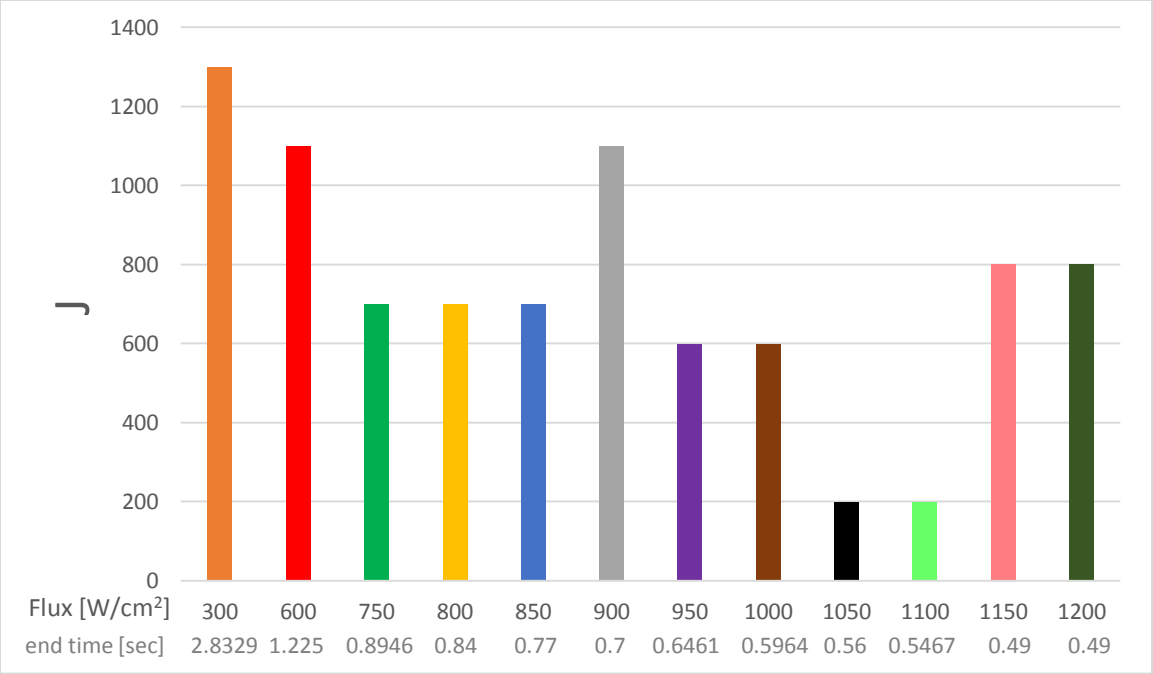

Figure 10: Plot of objective function values versus various flux values at respective ablation end times. A surface tension of 1 N/m, a mobility of 1 m•s/kg and a total element distribution of 960 elements were used.

To develop the objective function, relative weights were determined for ablation time and the total damage in the surrounding tissue. The total damage of the surrounding bone was given a maximum weight of 1000 while the total ablation time was given a maximum weight of 300. The sum of these give a total maximum optimization score (J) of 1300. With this optimization structure, the best model(s) would have the lowest optimization scores. As demonstrated by the bar chart above (Figure 10), a flux of 300 W/cm^2 received a maximum score as the model had the most amount of damaged tissue in the surrounding bone and the longest ablation time. Using this objective function, fluxes within the range of 1050 to 1100 W/cm^2 were the most optimized as these models had a relatively short ablation time (0.49 to 0.5467 seconds) and the lowest amount of surrounding thermal damage leading to a total ablation score of 200, the lowest of the models tested.

Conclusion

Model Evaluation and Implications

The model effectively demonstrates an inverse relationship between the flux of the laser and the total ablation time and a direct relationship between the flux and the total injury in the surrounding tissue. These results allow researchers to choose the flux range that finds a balance between the total ablation time and the possible tissue damage in the nearby area. Finding this balance is important such that injury in the surrounding bone may lead to loosening of the implant or refracture in the bone, while an extended ablation time may lead to increased risk of the surgery.

As a whole, this model also illustrates that laser ablation is a viable alternative to mechanical bone drilling. While drilling of the cortical bone takes approximately 18 seconds for a 6 mm hole, laser ablation, even at the lowest flux tested in this model, takes less than 3 seconds for the 5 mm hole (Augustin et. al., 2012). This reduced drilling time will amount to less time on the table for the patient which lessens the risk of infection. From this point, the laser demonstrates a clear advantage.

Non-contact laser ablation of the bone also reduces the amount of surrounding thermal damage as friction is greatly decreased. (Augustin et. al., 2012). An increase in drilling speed is associated with a significant change in the temperature of the surrounding tissue due to the frictional increase as well as the increase in drill pressure. With lasers however, drill pressure does not play a role in surrounding thermal damage, thus another main contributing factor is nullified. Overall in both aspects of the measured values, the laser-ablation is an advantageous method.

Constraints and Limitations

There are two main limitations in this model: the assumption that the scanning speed and the pulse duration are negligible and the assumption that the bone is isotropic. While significant, these limitations can be addressed in future work.

The main limitation of the model is the assumption that the scanning speed and the pulse duration of the concentric circle pattern are negligible. Because a continuous point flux was assumed instead, thermal damage and end time are thus slightly altered. With a pulsing flux, the thermal damage to the surrounding tissue would be reduced as the surrounding bone would have more time to cool but the total ablation time would also be greater as the time between the pulses that allowed for the cooling of the bone would remain unaccounted for in this model.

Another limitation of this model is that it can only be applied to homogenous, isotropic materials. In reality, the glenoid is anisotropic and its material properties vary depending on the orientation to which the force is applied (Frich et. al., 1997). Because the glenoid is anisotropic, the effects of the ablation of the bone will vary depending on the specific bone properties of an individual as well as the direction in which the bone is ablated, as that may also vary as individuals have their own bone structure.

Design recommendations

Despite these constraints and limitations, the practicality of laser ablation as an alternative to mechanical drilling should still be considered and studied further. From this model, a laser flux range within 1050 to 1100 W/cm^2 would be recommended for the ablation of a 5 mm deep hole. Though this model reduces the amount of experimental testing needed to demonstrate the CO_2 laser as a reasonable alternative to mechanical drilling, further research is still necessary. In addition to a modeling method with greater computing ability that will allow for femtoseconds and microsecond laser pulses to be applied, more research should be done on the anisotropy of the glenoid and how these properties vary throughout the population. More advanced modeling computation can decrease the amount of experimentation that will be required. Constraints to studying laser bone ablation include limited access to human bone and possible large-scale costs to purchase an accurate and precise CO_2 laser. Increased information about the thermal reactions inside the bone will thus allow researchers to better determine whether or not laser ablation will become the standard for the medical field in the future.

Appendix A: Mathematical statement of the problem

Governing Equations in COMSOL

As mentioned above, implementation of the laser ablation process in COMSOL required the use of a phase field equation in order to monitor the air-bone interface. The governing equation for the phase field equation is listed below:

$$\frac{\partial \emptyset}{\partial t} - m\delta\left(\frac{V_{f1}}{\rho_{air}} + \frac{V_{f2}}{\rho_{bone}}\right) = \nabla \cdot \frac{\gamma\lambda}{\varepsilon^2}\nabla\psi \tag{1}$$

where $\emptyset$ is the dimensionless phase field variable such that $-1 \leq \emptyset \leq 1$;, V_{f1} is the volume fraction of air and V_{f2} is the volume fraction of bone;, the quantity λ is the mixing energy density (N) and ε is a capillary width that scales with the thickness of the interface (m) that can be calculated by $\varepsilon = \frac{thickness\ of\ interface}{number\ of\ elements}$

To implement this equation, boundary conditions are needed. Listed below are the boundary conditions corresponding to the phase field model. First, the speed at which the interface moves is defined as follows:

$$\boldsymbol{u}_{int} = -\frac{m}{\rho_L}\boldsymbol{n} \tag{2}$$

Where $\boldsymbol{u}_{int}$ is the interface velocity; n is the unit normal vector to the interface directed from the bone phase to the air phase.

To calculate other parameters used in the phase field model including specific heat, the relationship between apparent specific heat and the specific heat capacity of the bone were defined as follows:

$$C_{pa} = C_{ps} + \frac{dm}{dT} \times 8.4 \times 10^6 \tag{3}$$

C_{pa} is the apparent specific heat capacity of bone and C_{ps} is the specific heat capacity of bone. In addition to this, the thermal conductivity and specific heat capacity are computed as functions of the volume fraction of the two phases:

$$\mathrm{k} = (k_s - k_g)V_{f2} + k_g \tag{4}$$

Where k_s is the heat conductivity of bone; $k_g$is the heat conductivity of air; V_{f2} is the volume fraction of bone;

$$C_p = (C_{pa} - C_{p\_g})V_{f2} + C_{p\_g} \tag{5}$$

C_{pa} is the apparent specific heat capacity of bone; $C_{p_g}$is the specific heat capacity of gas; V_{f2} is the volume fraction of bone. The surface tension coefficient is proportional to the mixing energy density indirectly proportional to capillary width that is related to the thickness of the interface.

$$\sigma = \frac{2\sqrt{2}}{3}\frac{\lambda}{\varepsilon} \tag{6}$$

In this relationship, σ is the surface tension coefficient; λ is the mixing energy density (N) and ε is a capillary width that scales with the thickness of the interface (m) that can be calculated by

$$\varepsilon = \frac{thickness\ of\ interface}{number\ of\ elements}$$

Relating these parameters back to the mass loss, the equation for the mass flux for the bone ablation is:

$$\dot{m} \approx C\rho_{bone}\left(\frac{T-T_{sat}}{T_{sat}}\right) \tag{7}$$

Where C is a constant (m/s). This expression is analogous to specifying a heat transfer coefficient on an external boundary of a heat transfer problem.

The thermal properties of bone, variables and laser parameters used in the equations above are described in Table A1 below.

Input Parameters

Table A 1: Summary of Parameters. The below variables were implemented in COMSOL model for solution.

Definition	Variable/ Parameters	Value	Units	Source
Saturation temperature at which we assume bone is loss	T_sat	613	K	(Lozano, 2013)
Constant in expression for mass flux	C	0.03	m/s	(Boiling Water)
Atmospheric Pressure	p0	101325	Pa	(Boiling Water)
	W	0.65		
Specific heat capacity of bone	Cps	1.254	J/(g·K)	(Clattenburg and Cohen, 1975)
Density of bone	rho2	1.91	g/cm^3	(Forrer, 1993)
Thermal Conductivity of Bone	Ks	6e-3	W/(cm·K)	(Forrer, 1993)
Laser Flux	q0	Variable (300, 600, 750, 800, 850, 900, 1000, 1050, 1100, 1150, 1200)	W/cm^2	N/A
Molecular Weight Of Water	Mw	0.018	kg/mol	(Boiling Water)
Specific Heat of air	Cp_g	1840	J/(kg·K)	(Boiling Water)
Surface Tension Coefficient	σ	Variable (0.1, 1, 10)	N/m	(Boiling Water)
Mobility	γ	Variable (0.1, 1, 10)	m·s/kg	(Boiling Water)

Appendix B

Mesh Creation and Convergence

When constructing the mesh for the model, a relatively large number of elements are needed to guarantee precision, especially because this model simulates an ultra-fast process in which major changes can occur within an extremely short time period. However, the larger the computational domain, the greater the requirement for computation memory and time. Therefore an ideal mesh would be one with enough elements to guarantee precision while minimizing computational time. A coarser mesh can be used in the surrounding tissue region without sacrificing accuracy of the simulation; a finer mesh should be used in the desired ablated area, especially at the air-bone interface, where the largest change occurs.

A structured mesh was applied to the entire desired ablated area. Also, an adaptive mesh was added to the structured mesh to increase accuracy of computation. The adaptive mesh allowed for the movement of a finer mesh to follow the air-bone interface where the transition from bone to air was taking place as can be seen below in Figure B1. The entire structured mesh was doubled. At the bone-air interface, where the largest change occurs, the mesh was doubled again, resulting in four times the initial mesh. A coarse free-triangular mesh was applied to the surrounding area. An unstructured mesh was used here because it is more flexible in fitting the surrounding domains and can provide rapid grading from large elements at the boundary to small elements outward.

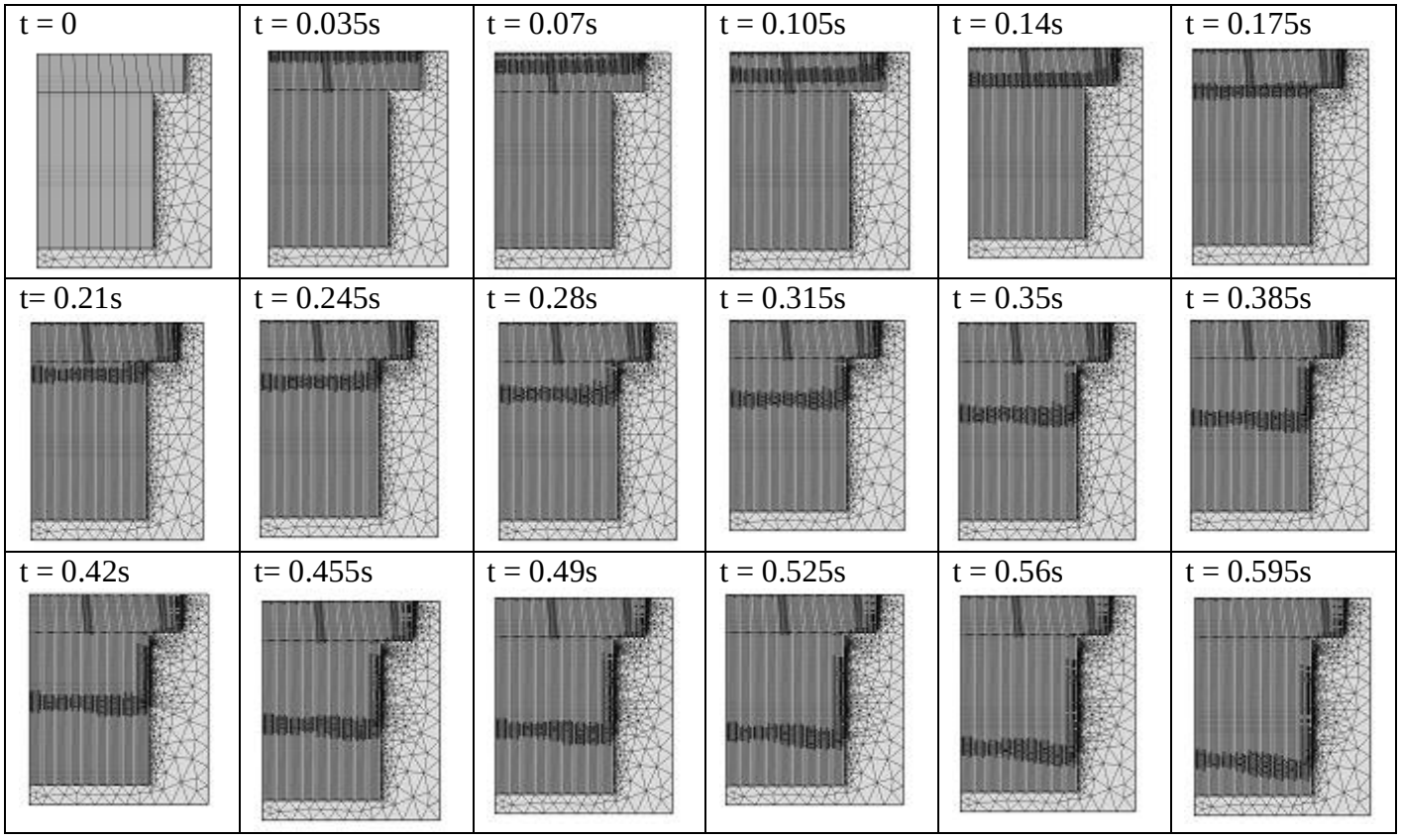

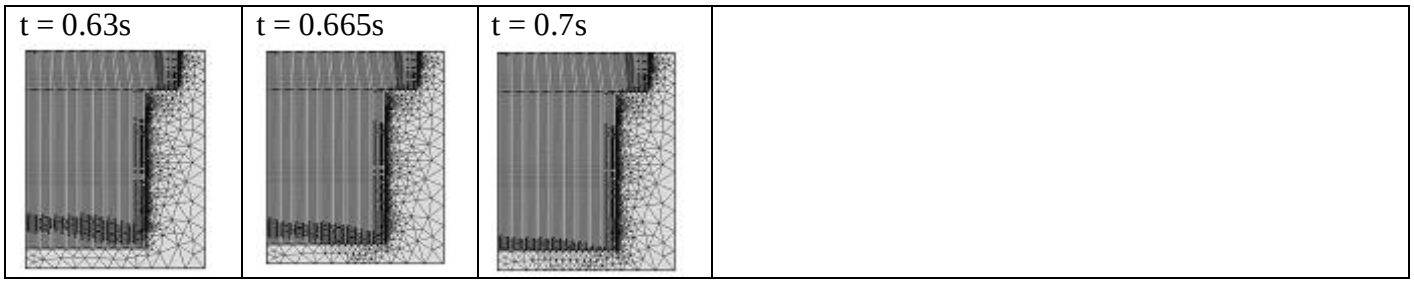

Figure B1: Schematic of the adaptive mesh over time. For demonstration purpose, a time step of 0.035s and a time of 0.7s were used. A total element distribution of 960 elements was implemented to account for the structured mesh in the ablated region.

To determine the mesh that would be used to run the model, a mesh convergence was performed in which the number of elements in the adaptive mesh varied from 480 to 2400 demonstrated in Figure B2.

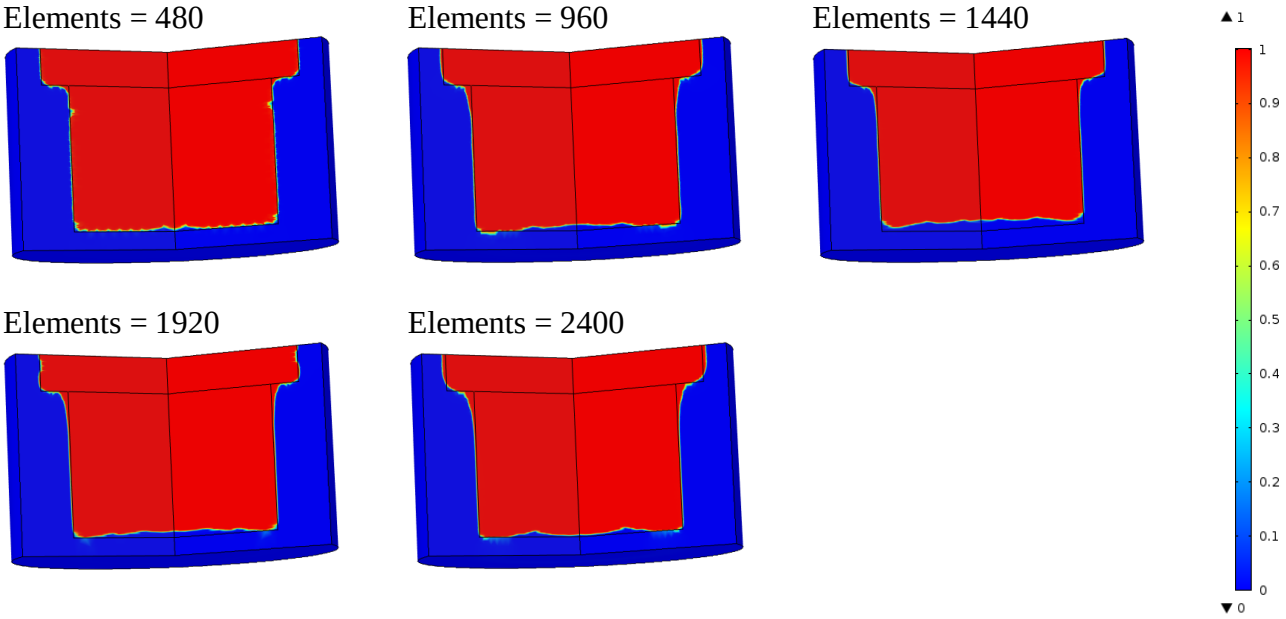

Figure B2: The effect of various number of meshing elements on the bone-air interface. Color scale of Air volume fraction (Vf1). The mesh chosen in the model is justified by testing for convergence of air fraction volume result values. This number was determined by experimentation with the model; various element distributions were run with the desired model parameters. For this model, total element distributions of 480, 960, 1440, 1920 and 2400 elements are implemented in the ablated region. Air fraction of the surrounding tissue in the model was observed to determine mesh convergence. A 2-D surface plot of total air volume for each element distribution is shown for reference in Figure B1.

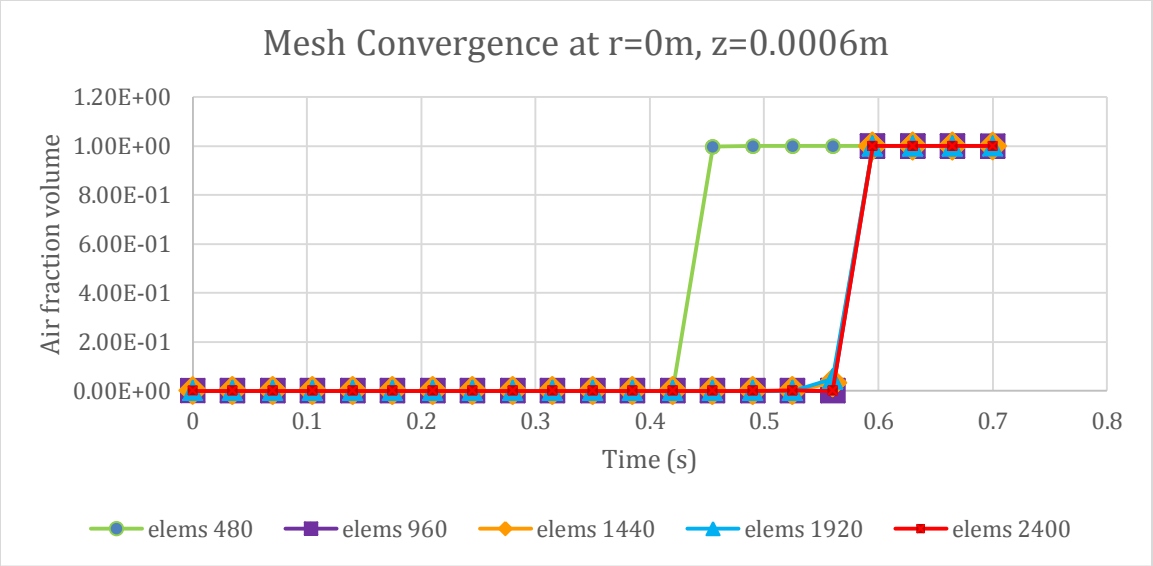

Figure B3: Air fraction volume (Vf1) versus time with various element numbers at r = 0 m, z = 0.0006m. As seen in the air fraction volume over time at the location r=0m and z=0.0006m, mesh two through five display relatively similar results while mesh one show shifted results, which indicates that mesh converges at the element number of 960. Because mesh two is sufficient to achieve a precise enough result, it was chosen to run the computational experiments.

Appendix C: Additional Visuals

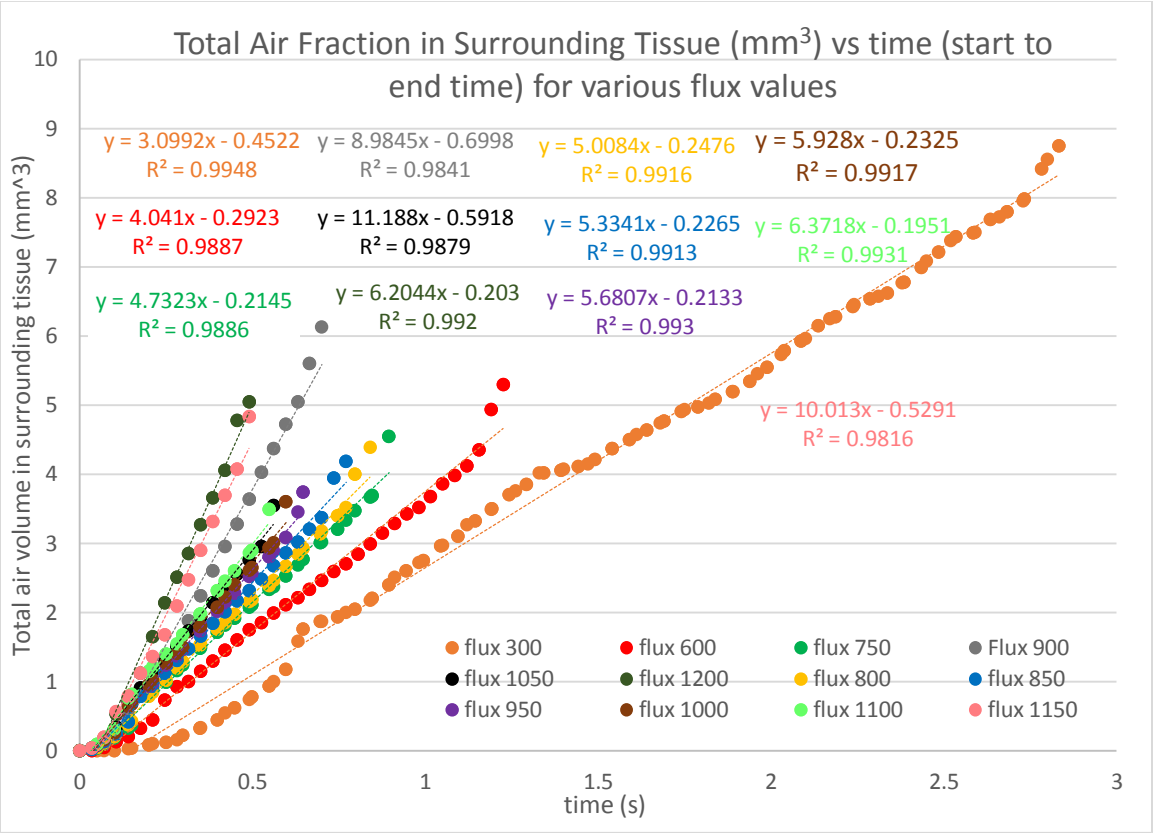

Figure C1: Total Air volume in Surrounding Tissue (mm^3) vs. ablation time for various flux values. A surface tension of 1 N/m, a mobility of 1 m·s/kg and a total element distribution of 960 elements were used.

The total air fraction values were obtained by integrating the air fraction volume (Vf1) over the surrounding area. Total air fraction in surrounding tissue represents disintegration of bone, thus can be used as to measure the extent of thermal injury.

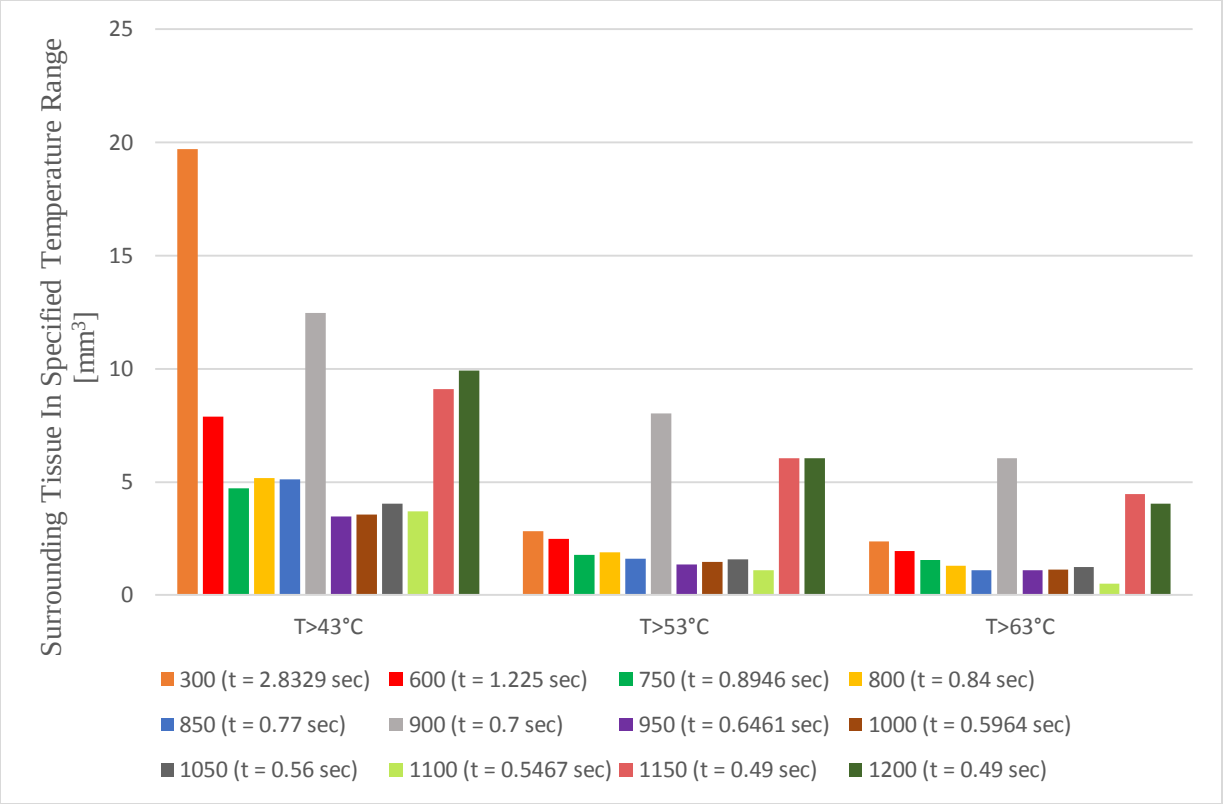

Figure C2: Surrounding tissue volume in specified temperature range for varying fluxes. Normally body tissue is injured when exposed to a temperature over 43℃ at a long time. Therefore, T > 43℃ was used as one of the criteria to study thermal injury. However, the ablation processes were done within a few seconds, so that higher temperature ranges, including T > 53℃ and T > 63℃ were also considered.

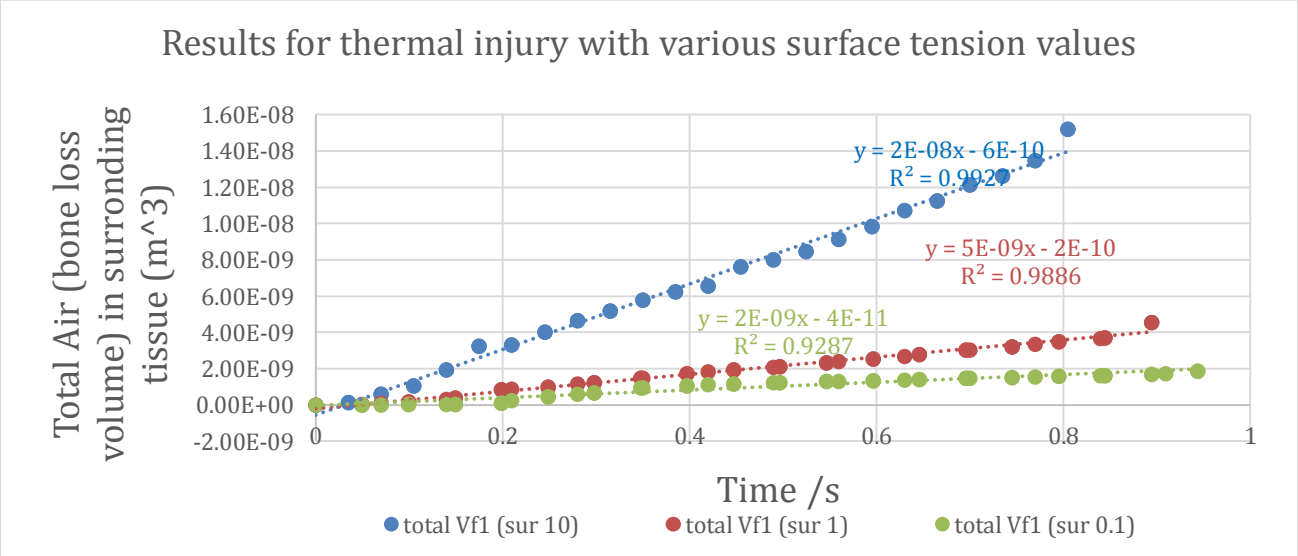

Figure C3: Total Air Volume in surrounding tissue versus time with various surface tension coefficients.

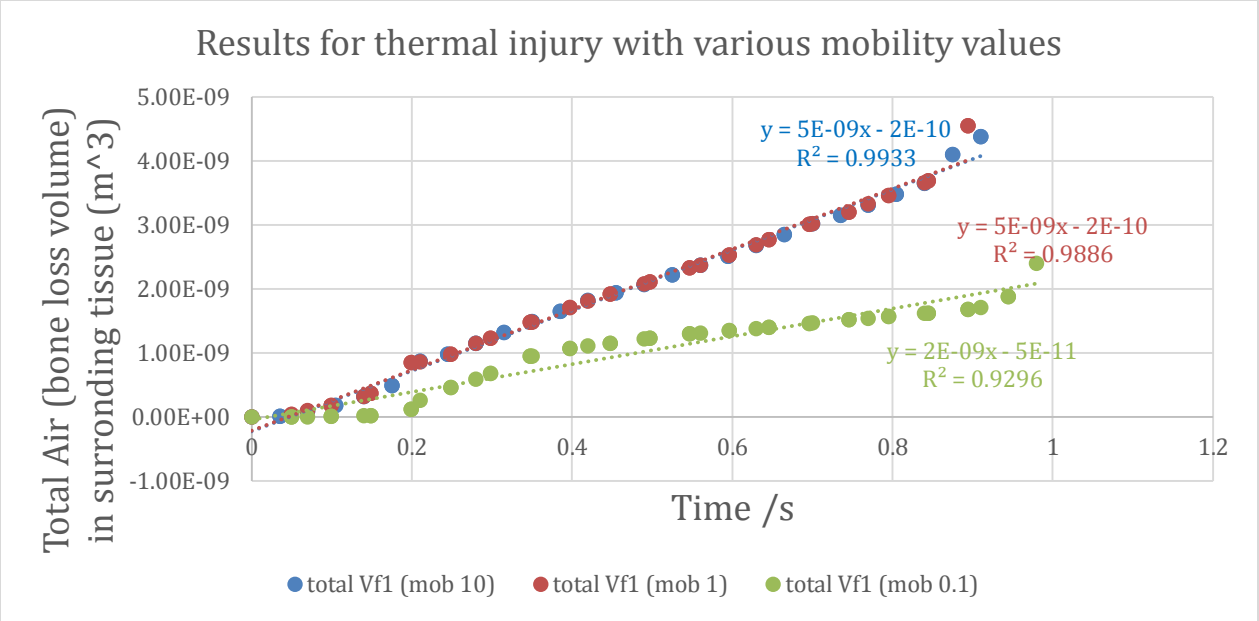

Figure C4: Total Air Volume in surrounding tissue versus time with various mobility coefficients.

Slope value of average volume fraction of air (average Vf1) reflects the rate of ablation at the end time steps, and therefore can be used as an indicator of how sensitive the process is in response to the input parameters. According to figure 7, volume fraction of air in the ablated area is more sensitive to the change of flux and surface tension comparing to that of mobility.

Appendix D: References

Augustin, G., Zigman, T., Davila, S., Udilljak, T., Staroveski, T., Brezak, D., & Babic, S. (2012). Cortical bone drilling and thermal osteonecrosis. *Clinical Biomechanics, 27*, 313–325.

Bertollo, N., Walsh, W. (2011). Drilling of bone: practicality, limitations and complications associated with surgical drill-bits. ISBN 978-953-307-969-1

Boiling Water. n.d. Web. 19 March 2014. <http://www.comsol.com/model/boiling-water-3972>.

Calttenburg, R., Cohen, J., Conner, S., & Cook, N. (March 01, 1975). Thermal properties of cancellous bone. Journal of Biomedical Materials Research, 9, 2, 169-182.

Emigh, B. J. (2011). Experimental Evaluation of Bone Drilling using Ultrashort Pulsed Laser Ablation.

Forrer, M., Frenz, M., Romano, V., Altermatt, H. J., Weber, H. P., Silenok, A., Konov, V. I. (1993). Bone-ablation mechanism using CO 2 lasers of different pulse duration and wavelength. *Applied Physics B-lasers and Optics, 56*, 104-112.

Frich, L. H., Jensen, N. C., Odgaard, A., Pedersen, C. M., Søjbjerg, J. O., & Dalstra, M. (January 01, 1997). Bone strength and material properties of the glenoid. *Journal of Shoulder and Elbow Surgery / American Shoulder and Elbow Surgeons ... [et Al.], 6*, 2.)

Ivanenko, M. M., & Hering, P. (1998). Hard tissue ablation with a mechanically Q-switched CO2 laser. *Thermal Therapy, Laser Welding and Tissue Interaction*, SPIE Proc.. vol. 3565, 110-115. doi:10.1117/12.335790.

Lozano, L. F., Pena-Rico, M. A., Heredia, A., Ocotlan-Flores, J., Gomez-Cortes, A., Velazquez, R. Bucio, L. (2003). Thermal analysis study of human bone. *Journal of Materials Science, 38*, 4777 – 4782.

Niemz, M. (1996). Laser-tissue interactions: Fundamentals and applications.Springer-VerlagBerlin and Heidelberg, GmbH & Co. ISBN: 978-3-540-72191-8